Improved Controllability of Opal Film Growth Using Capillaries for the Deposition Process

Hong-Liang Li, Wenting Dong, Hans-Josef Bongard, and Frank Marlow*

Max-Planck-Institut für Kohlenforschung, Kaiser-Wilhelm-Platz 1, 45470 Mülheim an der Ruhr, Germany

Received: January 21, 2005; In Final Form: March 24, 2005

A capillary deposition method for the preparation of opal and inverse opal films has been developed. By this method, one can control the film thickness and the crack arrangement in opal as well as inverse opal structures. This method combines tube capillarity with cell capillarity or with gravity depending on the stability of the suspensions. The combination of tube capillarity with cell capillarity is used to prepare opal films from stable suspensions. The tube capillary transports the suspension, while the cell capillary helps to assemble the spheres. The setup defines the drying fronts, thickness, and crack arrangements of the opal films. The combination of capillarity with gravity is useful for making opal films from unstable suspensions. Opal films of spheres with size up to 1 μm can be easily prepared from this combination. Here, the gravity influences the arrangement of the spheres. The two-capillary setup has also been used to infiltrate the opal films with a titania precursor. After calcination, inverse titania opal films with skeleton structure have been obtained.

1. Introduction

The concept of photonic crystals (PhCs) became well known since Yablonovich and John introduced the idea that PhCs can confine and control light and its emission.[1,2] Up to now, two basic concepts have been documented for building three-dimensional PhCs. The first one is to exploit the traditional techniques that have been applied in the processing of semiconductors. The second approach uses a self-assembly of nano- or microsized units, such as semiconductor[3] or other small particles. A popular self-assembly method for fabricating colloidal crystals is the gravity sedimentation of colloids from dispersions.[4−6] This method produces thick opals and can be altered in different ways depending on the pursued goals. However, the natural sedimentation methods usually will generate samples with polycrystalline domains of unknown sizes.[7,8] In addition, the method can only be used for colloids of specific spheres.[4] When beads are too small or too large, bad quality or no sedimentation is achieved in a reasonable time.[6]

Strong capillary forces at a meniscus between a substrate and a colloidal sol can induce crystallization of spheres into a 3D array of controllable thickness.[9−11] If this meniscus slowly swept across a vertically placed substrate by solvent evaporation, thin planar opals can be deposited.[12] This normal vertical deposition method (or convective self-assembly) is believed to be limited to spheres with diameters <0.4 μm because of the competition between the solvent evaporation and the sphere sedimentation.[13] To extend the applications of this promising method, several groups have contributed modifications.[13−15] Mechanical agitation by controlled gentle stirring was utilized successfully by Ozin and co-workers for crystallization of large silica spheres within surface relief patterns in optical microchips.[16] However, it did not work well for the preparation of continuous colloidal crystal films because the swirl created by stirring disturbs the meniscus and impedes successful growth of continuous colloidal arrays. Furthermore, a convective flow was added to the deposition process, and colloidal crystals consisting of large-sized silica spheres (up to 1 μm) have been deposited.[13,15] The required conditions, such as the temperature control, turned out to be very critical for opal film preparation from unstable suspensions.[15,17]

When opals are grown on solid substrates by a self-assembly process, drying leads to crack formation because of the contraction phenomena.[18] An ingenious way to circumvent this problem is to perform the growth on a liquid surface. Using this method, millimeter-wide crack-free samples have been prepared in Zentel's group.[19] However, it seems to be not possible to avoid the cracks on solid supports. One challenge for the fabrication of PhCs using the spontaneous crystallization of colloids is the creation of PhCs with intentional defects that allow photon states within the band gap.[20,21] Unfortunately, shrinkage usually will result in disordered defects, destroying the effects of the intentional defects.[20]

A creative way to growing opal films in a confinement cell has been developed by Xia et al.[22] The confinement cell consists of two glass slides separated by a lithographically defined resist in the shape of a rectangular frame with draining channels. After injecting the suspension into the cell, opal films with controlled thickness can be produced. However, the cell preparation requires complicated lithographic facilities and very good manual skills, which limit the flexibility of the method, and it is difficult to perform in a usual chemical laboratory.[14]

The infiltration with materials of high enough refractive index can convert opals into interesting structures, because inverse opals can sustain a complete photonic band gap.[23] The templating method has been demonstrated to be a promising approach to the fabrication of three-dimensional inverse opals.[24−26] First, the opal templates are infiltrated with a liquid precursor of the inverse structure. Usually, concentrated precursor is needed; otherwise, many infiltration cycles become necessary, even though it is difficult to control the homogeneity of the infiltration.[27]

It has also been shown that in the inverse opals fabricated via a sol−gel method, three different structures can occur: residual volume structures, shell structures, and skeleton

* Corresponding author. Phone: 0049-208-3062407. Fax: 0049-208-3062995. E-mail: marlow@mpi-muelheim.mpg.de.

10.1021/jp050385d CCC: $30.25
Published on Web 04/23/2005

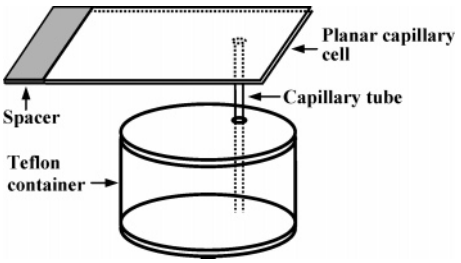

Figure 1. Setup used for the preparation of opal films from stable PS colloids. The dark area inside the planar capillary cell shows the spacer; the other three sides are open.

structures.[28] The skeleton structure shows very interesting properties such as two complete band gaps contrary to common inverse opals where only one band gap occurring between the eighth and ninth bands is found.[29] However, the exact control of the inversion process is still a challenging issue.[28,30]

Here, we are reporting on a capillary-assisted method for the preparation of opal films and inverse titania opal films. It has the following merits: (1) The use of two different capillaries to convey and to assemble the spheres, respectively, avoids the competition between the sphere sedimentation and the opal deposition. This extends the application of capillarity in opal film preparation. (2) It is easy to operate and can be applied to different-sized polystyrene, silica, and other particles, while it is not important if their suspensions are stable or not. (3) It results in large-area opal films (more than 3.5 cm^2), while the directions of the cracks in the films can be controlled by modifying the experimental setup. (4) The setup is also useful for the infiltration of opal films with liquid precursors. By infiltrating the opal films with liquid precursors, large area inverse opal films with skeleton structure have been fabricated after calcination.

2. Experimental Section

Materials. Suspensions of 10 wt % polystyrene (PS) spheres with different radii (deviations smaller than 3%; Duke Scientific), silica spheres (radius deviations smaller than 5%, monosphere, Merck), and titanium iso-propoxide 98% (Aldrich) were used as received. The silica spheres were dispersed into deionized water with the assistance of an ultrasound bath, forming a 0.5 wt % suspension. Normal glass slides and glass slides with a 1 mm hole at different positions were immersed in 5% Labosols (Neolab) aqueous solution and in 0.5 M NaOH ethanol/water (1:3, V/V) solution for 0.5 h, respectively, and then rinsed with deionized water completely. After that, the slides were dried under an air flow. Capillary tubes with a 1 mm external diameter and 20 mm length have been used.

Construction of the Planar Capillary Cell. Two glass slides with the same size, one of them with a 1 mm diameter hole, were separated by a strip of thin spacer, forming a planar capillary cell. The spacer can be a polymer or metal layer. It does not matter which kind of material is used; however, they should be robust and with suitable thickness. In our preparation, a polymer film (Super 200, Gelman Sciences) with a thickness of about 75 μm has been utilized. The edges of the cell have been left open or closed depending on the experimental purposes.

Opal Film Growth. The capillary tube was connected to the capillary cell via the hole on the bottom slide without any glue, only by a good fitting of the tube inside the hole. The open end of the tube was inserted into the PS suspension within a Teflon container. Figure 1 shows the setup that has been used for the making of opal films from 0.26 and 0.5 μm PS sphere suspensions. Here, the capillary cell is horizontal. Due to the capillarity, the suspension in the Teflon container filled the capillary tube, and then it was relayed by the capillarity of the two-slide capillary cell and filled the void. The suspension started to solidify along the open edges, and then filled the cell with spheres within several days, forming a solid opal film. The experimental setup has also been applied to make opal films from large-sized sphere suspensions, but the planar capillary cell is tilted by about 15° to the horizon.

Inverse Opal Preparation. The same setup as shown in Figure 1 has been used for the infiltration of opal films by replacing the suspension inside the Teflon container with a liquid precursor, for example, a titanium iso-propoxide ethanol solution. The infiltration was carried out inside an Ar flow protected desiccator or in the air. After the infiltration, the film was exposed to air for 1 week to hydrolyze the iso-propoxide. To remove the PS template and crystallize the oxides, the films were heated to 500 °C in the following way: 0.44 °C/min to 80 °C, 1 h at 80 °C, 1.33 °C/min to 200 °C, 1 h at 200 °C, 1.67 °C/min to 500 °C, 3 h at 500 °C, and then cooled to room temperature.

Characterization. The overviews of the films were recorded with a Casio digital camera. A Leitz Orthoplan microscope was used for the optical microscopy images. SEM was measured on a Hitachi S-3500N scanning electronic microscope. The optical quality of the opal films was investigated with a Cary 500 UV−vis−NIR spectrophotometer in transmission mode.

3. Results and Discussion

3.1. Principle of the Method. The method for the preparation of opal films described in this work is called bi-capillary deposition method. The operation principle differs slightly for stable suspensions and unstable suspensions.

Figure 1 shows the setup, which has been used for the preparation of opal films from stable suspensions. The capillary tube absorbs the suspension when it was inserted into a suspension. If the capillary tube is connected with a capillary cell, the capillary cell extracts the suspension from the capillary tube, and the suspension is conveyed from the container into the whole capillary cell and stops at the edges. Thereafter, the solvent evaporates through the open sides, and the capillary force continues the suspension delivery. The spheres remain and assemble along the open edges. After the capillary cell is filled with spheres, the film dries because no suspension can enter the cell any more and the diffusion of the solvent alone is too slow.

For unstable suspensions, the planar capillary cell was titled about 15° to the horizon (see Figure 6). Now, the sedimentation by gravity contributes to film formation, instead of competing with it. The capillary tube and the capillary cell have the same delivery functions as in the stable suspension case. Because the sphere suspension is unstable and the capillary cell is tilted, the spheres inside the capillary cell move preferentially to the lower part of the cell and start to deposit from there until the spheres fill the whole space of the cell. During the deposition process, the unstable suspension inside the Teflon container is stirred with a magnetic stirrer to avoid sedimentation. This agitation does not influence the film deposition inside the capillary cell because the suspension inside the container is separated from the capillary cell via the capillary tube.

The opal films prepared by this method are summarized in Table 1. All of the prepared films show homogeneous and angle-dependent colors. They are very stable and easy to handle as long as the opal films remain between the two glass slides. No

TABLE 1: Relationship between the Sphere Diameter, Suspension Concentration, Film Growth Velocity, and the Distance between the Cracks for PS Opals[a]

sphere diameter (μm)	suspension concentration (wt %)	growth velocity (mm/day)	distance between the cracks (mm)	film color diffuse/0° reflected
0.26	2	3.5	0.12−0.16	light turquoise/copper
0.26	1	2.0	0.12−0.16	light turquoise/copper
0.26	0.5	1.0	0.12−0.16	light turquoise/copper
0.26	0.25	0.6	0.12−0.16	light turquoise/copper
0.50	0.5	1.2	0.22−0.26	white/white
0.93	0.5	1.0	0.35−0.50[b]	white/white

[a] The film color depends on the illumination. The appearance with diffuse white light and normal-incidence reflected white light is described. [b] The opal films of 0.93 μm PS have large free regions, but also regions with ordered cracks.

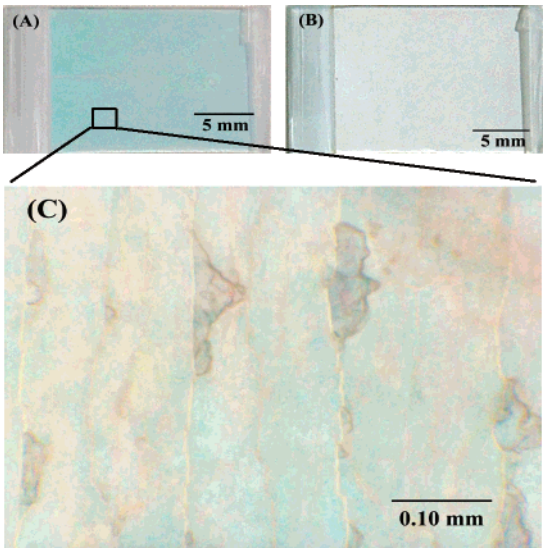

Figure 2. Overviews of an opal film consisting of 0.26 μm PS spheres (A) and an opal film made from 1.0 μm silica spheres (B), and an optical microscopy image (C) of a selected area in image A.

sintering of the opal spheres is required. The suspension concentration affects the film growth speed (see Table 1), but not the film thickness as in the vertical deposition method.[12] The thickness of the opal film is determined by the spacer between the two slides and can be easily tuned. The distance between the cracks is not influenced by the suspension concentration. However, it increases with the increase of the sphere size.

3.2. Crack Alignment. Pictures A and B in Figure 2 show the typical overviews of an opal film consisting of 0.26 μm PS spheres (A) and a film made from 1 μm silica spheres (B). Picture C is an optical microscopy image of the same film as in picture A taken at the indicated position. It reveals linear-ordered cracks, which are perpendicular to the open long edge of the cell. The average distance between two cracks is about 0.14 mm. A similar result has been obtained for opal films of 0.5 μm PS spheres, while the average distance between the cracks increased to about 0.24 μm (see picture E of Figure 3). However, in opal films of 0.93 μm PS or of 1 μm silica, only a few regions have regular crack arrangement, but they also show large area (about 1 cm^2) without cracks.

Different crack arrangements (pictures A, B, C, E, and F in Figure 3) have been obtained by modifying the boundary conditions of the planar capillary cell as it will be discussed in the next chapter. The opal films prepared from stable suspensions have all in common that the cracks are perpendicular to the open edges of the cell. They have a nearly fixed distance, which is independent of the concentration of the suspensions (see Table 1). Such a regular crack arrangement as described here has not been reported for the other opal preparation methods. The regularity seems to be connected with the specific drying process in the capillary cell and might be explained by the following hypothesis. The ordered solid arrangement of PS particles is already formed when the solid is still wet, that is, water-containing, which has been confirmed by optical transmission measurements of the wet films. The wet films show very pronounced Bragg peaks, indicating that the spheres are arranged regularly (see Figure S1). The main shrinkage problem therefore arises during a wet-solid to dry-solid transition. Because the particle movement in the solid is strongly suppressed, the PS/water system can only handle this problem by crack formation. In our setup, we have a clearly defined and slowly moving drying front. The front enables another solution for the system, a collective shift of the whole wet solid into the direction of the dry solid. The shift avoids the cracks parallel to the drying front, but not perpendicular to it. This process would, therefore, explain the observed crack pictures. Similar mechanisms have also been discussed for related drying phenomena.[31,32]

In the last paragraph, it has been assumed as in many other works that the cracks are formed during the drying process.[12] Here, we give a direct proof for this assumption (Figure 3, picture D). When we stopped the supply of the capillary cell with the suspension during the film growth and observed the wet film in-situ using an optical microscope, then we saw the crack formation after a few minutes. Picture 3D was taken in this moment. The cracks grew with a velocity of several mm/min, and they ended at the drying boundary.

It is interesting to compare our crack patterns with those of other methods. Therefore, pictures of two samples made by the well-known vertical deposition method from 0.5 and 1.0 wt % PS aqueous suspensions have been included in Figure 3 (pictures G and H). The cracks show grid-like patterns here, and the domain sizes of the two films made from different concentrations are different. Likely, this effect results from different sample thickness. In our capillary deposition method, the PS concentration influences the deposition speed but not the morphology of the films (see Table 1).

Figure 4A and B shows SEM top views of an opal film consisting of 0.26 μm PS spheres with different magnifications. From images A and B, we can see that the film is very smooth and exhibits an ordered close-packed arrangement of PS spheres over a sample width of larger than 100 μm, although small disturbances in the sphere positions are also visible. The disturbances can also form very small cracks or line-like defects, which are, however, smaller or comparable to the lattice constant. The main cracks are much larger than the lattice constant. The small cracks are seldom and depend on preparation details. Apart from the big cracks, which have already been discussed, the most frequent defects are the sphere vacancies as it is also known from similar samples.[19] A rough estimation of the concentration of the sphere vacancies results in 10^{-3} for

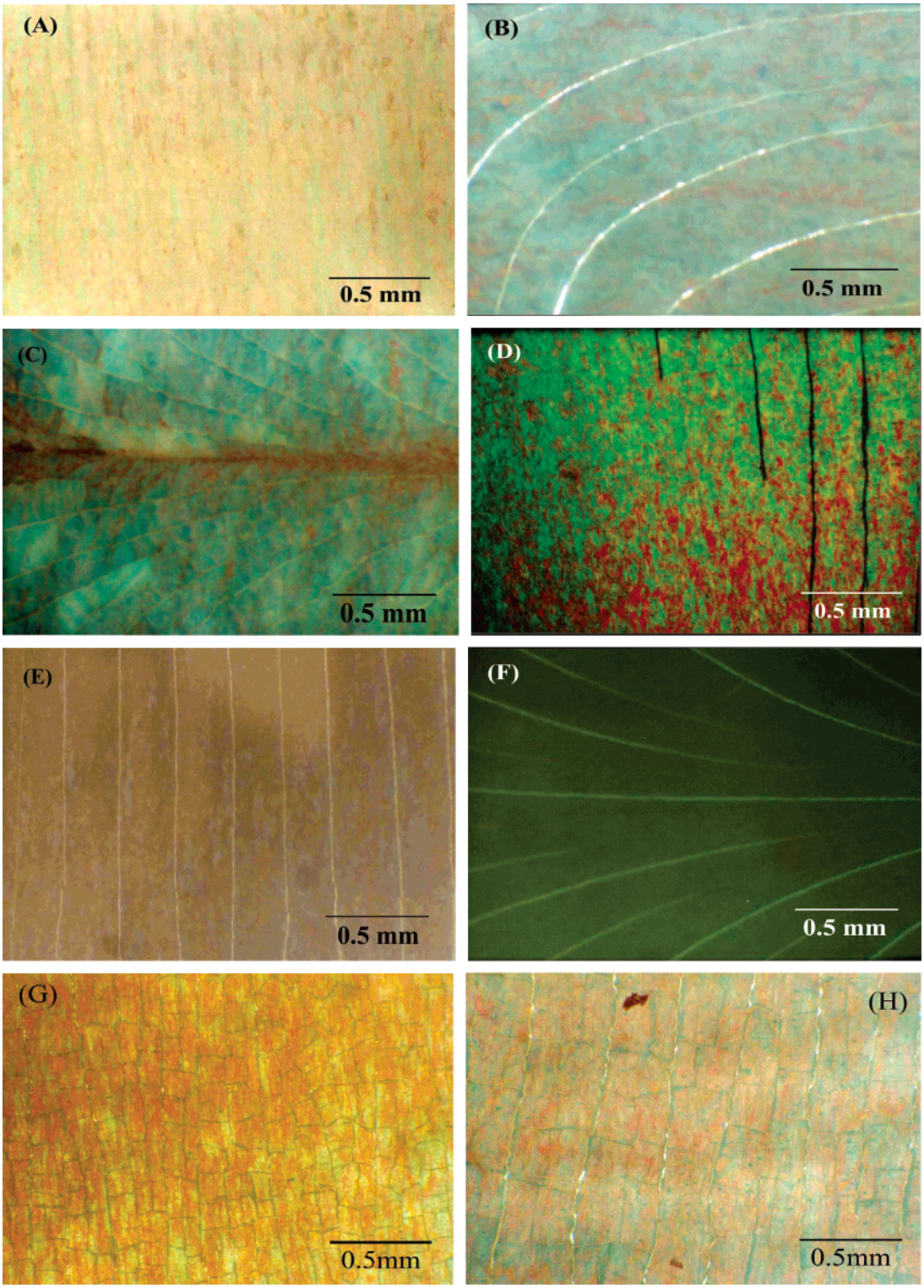

Figure 3. Opal films with different arrangements of cracks: (A) linear, (B) curved, and (C) fan-shaped. (D) Observation of the crack formation process during drying. These films are made from 0.5 wt % suspension of 0.26 μm PS spheres. Similar arrangements have been observed in opals film of 0.5 μm PS spheres, for example, (E) linear and (F) fan-shaped ones. (G) and (H) are images of opal films made by the vertical deposition method from 0.5 and 1.0 wt % suspensions of 260 nm PS spheres, respectively.

our samples. The drying process in thin colloidal films is also known from other works to cause cracks.[33] Our results show the same in thicker opal films. The addition of surfactants or a more detailed control over the drying conditions could be two possible strategies for minimizing this effect.

Pictures C and D of Figure 4 are cross-sectional images of the film under different magnifications. The low magnification image shows the film is homogeneous and with a thickness of the used spacer. The higher magnification shows the inner structure of the opal film, which is consistent with a well-ordered fcc packing of the spheres (for an enlarged high-resolution image, see Figure S2). Therefore, we conclude that this opal film prepared with the capillary deposition method is homogeneously ordered from the top to bottom.

3.3. Control of the Crack Arrangement. The boundary condition of the capillary cell is one of the factors that affects

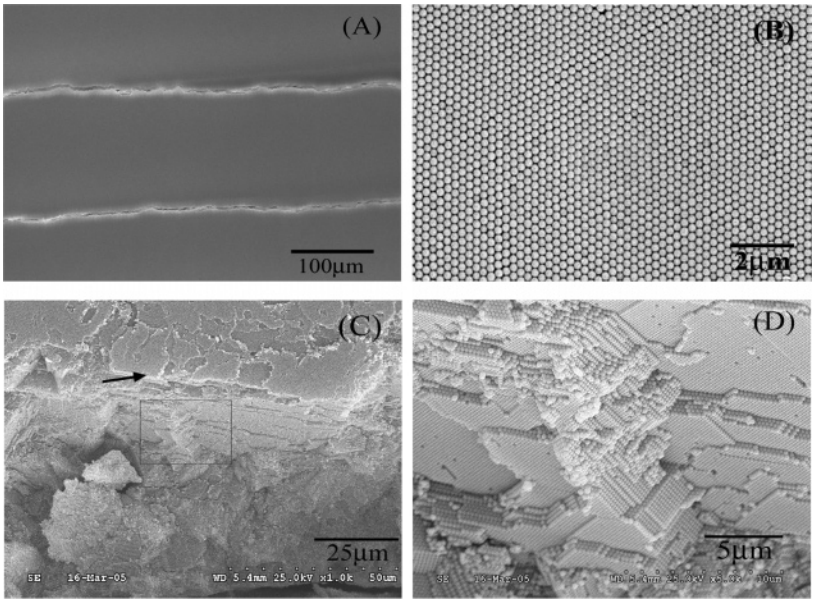

Figure 4. SEM top views (A and B) of the surface for an opal film consisting of 0.26 μm PS spheres, and views of a cross section with different magnifications (C and D). (The arrow in image C shows the upper edge of the opal film, and the rectangle shows the area in which image D was taken; an enlarged high-resolution image of picture D can be seen in the Supporting Information.)

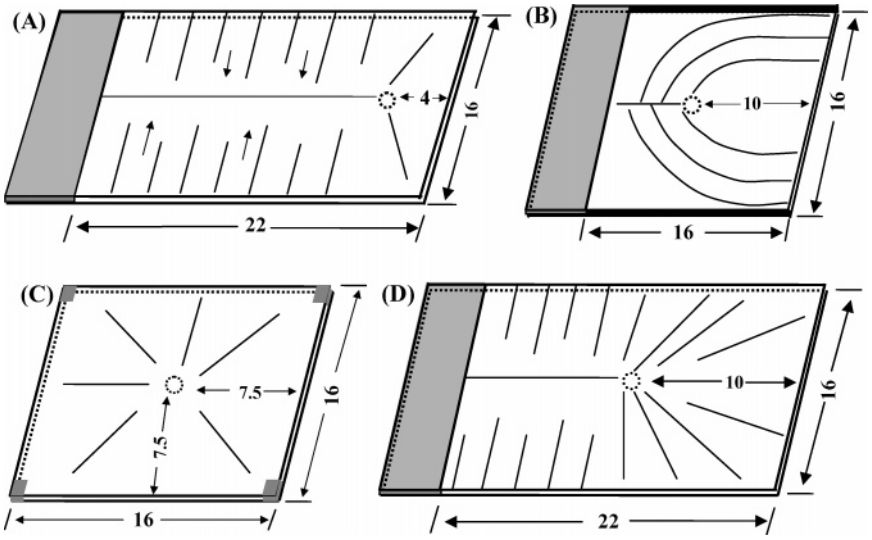

Figure 5. Schematic drawing of the relationship between the boundary conditions and the crack shapes. The black borders in (B) indicate the closing of the sides. The influence of the hole position on the crack shape is visible by comparing (A) and (D). All distances are in millimeters.

the crack arrangements. It influences the direction of the drying fronts and, therefore, the crack directions. We show the effect by three examples:

In a rectangle shape cell, cracks in linear shape have been obtained if three sides are opened (Figure 5, Scheme A). The arrows in scheme A show the film growth direction inside the capillary cell. If only one side is left open, then an opal film with curved cracks is obtained (Scheme B). When all four sides are opened, opal films with fan-shaped cracks are found (Scheme C). Because the film is dried through the open edges, blocking of the evaporation at different edges changes the solvent evaporation route, which determines the crack arrangements.

The second factor is the shape of the capillary cells. When a rectangle cell is applied, then we get opal films with linear shape cracks if we leave three sides opened, whereas we get more fan-shaped cracks if a square capillary cell is utilized.

A further factor for the arrangement of cracks is the position of the hole on the slide. If the hole lies at the center, the resulting film is divided into two parts with fan-shaped cracks and linear arrangement of cracks (scheme D). Therefore, a hole near the open edge was used if a film with more linear shape cracks was desired, while a hole at the center of a square capillary cell proved to be useful if an opal film with a fan-shaped crack arrangement should be obtained.

3.4. Unstable Suspensions. Usually, it is difficult to make opal films from large-sized spheres due to the low stability of their suspensions. By the capillary deposition method, it is, however, possible to prepare opal films from unstable suspensions as it has already shown in Figure 2, picture D. Figure 6 shows the setup scheme. For the operation principle, we refer to section 3.1. The opal deposition grew continuously from the bottom to the top until the spheres fill the whole space of the cell. After drying, a smooth opal film was obtained. The crack alignments in the opal films made from 1.0 μm silica and 0.93 μm sized PS are seldom visible.

SEM image A of Figure 7 shows a top view of a selected area of the opal film made of 1 μm silica spheres. An image size over 10^3 μm^2 can be easily obtained. There are some single

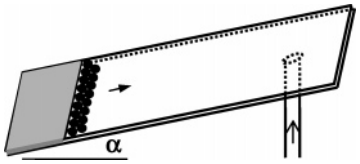

Figure 6. Scheme of opal film growth using an unstable suspension. For suspensions of 1 μm silica spheres or 0.93 μm PS spheres, a tilt angle α of about 15° has been used. The solid arrow shows the film growth direction; the open arrow indicates the suspension flow.

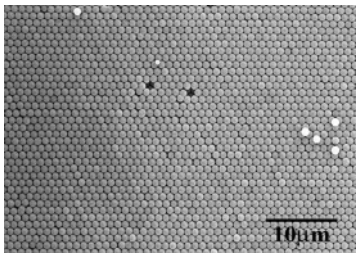

Figure 7. SEM image of an opal film made from 1.0 μm silica spheres.

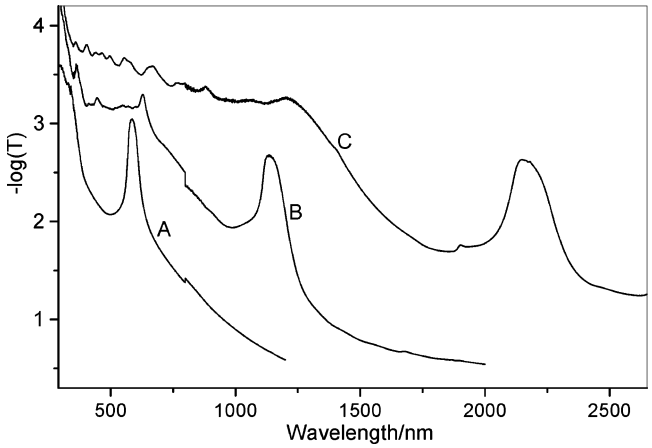

Figure 8. UV−vis−NIR transmission spectra of the opal films made of 260 nm PS (A), 500 nm PS (B), and 1000 nm silica spheres (C).

particles on the top of the film; likely they had been pulled out of the surface and jumped back to the surface during the separation of the slides, introducing more vacancies on the film surface.

3.5. Optical Properties. Figure 8 shows the typical UV−vis−NIR spectra of three films made of 260 nm PS, 500 nm PS, and 1000 nm silica spheres, respectively. The peaks in the spectra depend obviously on the sphere diameters as expected from the Bragg's law, and peaks centered at around 585, 1135, and 2170 nm have been observed for these three opal films. The high energy modulations in curves B and C might be higher order Bragg peaks. The presence of the high energy bands can be explained as due to a decrease in scattering of the samples originating from the perfection in the colloidal crystal order in the films.[15]

3.6. Infiltration of Opal Films. The same capillary setup has been used to infiltrate the dried opal films with a precursor solution for inverse opals, for example, the titania precursor of titianium(IV) iso-propoxide. There are two possible infiltration processes: the first one is carried out inside an Ar flow protected desiccator, and then the sample is exposed to the air to hydrolyze the precursor; alternatively, the infiltration is carried out in the air only by protecting the precursor inside the container with an Ar flow. The infiltration, concentration, and hydrolysis then take place at the same time. The first process is more defined because one can control different factors separately, while the

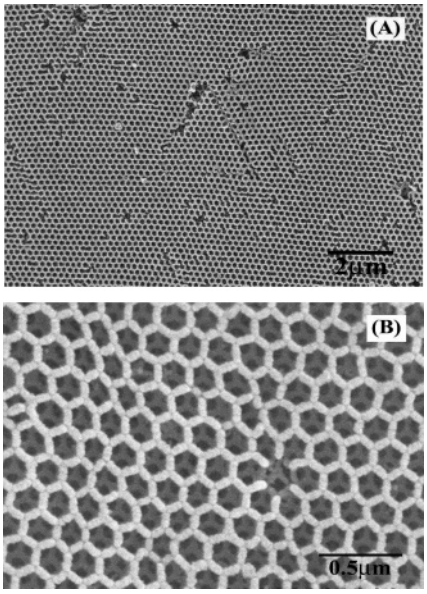

Figure 9. SEM images of inverse opal with different magnifications. Most of the point defects in the skeleton structure arise very likely during opening of the planar capillary cell, because their concentration is about 10 times higher than in the corresponding opals (1.2×10^{-2} in this sample).

second process saves the preparation time. The solution, which has infiltrated into the film, is then concentrated slowly upon the solvent evaporation, while the capillary tube compensates the solution loss continuously. The advantage of this bi-capillary-assisted infiltration method is that it does not have a special request for the concentrations of the precursor solution, and it infiltrates opal films homogeneously with the precursor. After calcinations, inverse opal films with skeleton structure are obtained. Pictures A and B in Figure 9 show the titania inverse opal film with different magnification. From image A, we can see that there are some defects inside the inverse opal film; however, the film is almost homogeneous. The high-magnification SEM image (picture B) shows clearly that the inverse structure is a skeleton structure.[29,30] This result reproduces the findings of ref 29. Additionally, it avoids a problem in this work. There, the skeleton structure was only found in the inner part of the opal pieces, demanding a rather complicated sample handling. Here, the skeleton structure is visible at every position except close to the borders. No indication for a shell structure has been found. At the border, the structure is not very well defined over some micrometers and allows no assignment to a specific inverse opal structure.

4. Conclusions

An opal and inverse opal preparation method based on capillarity and gravity has been developed. This bi-capillary deposition method improves the previously developed capillarity and gravity methods and makes them more flexible and robust. By combining tube capillarity with cell capillarity, one can easily prepare opal films from stable suspensions. This method has also been successfully applied to the preparation of opal films from unstable suspensions. In this case, capillarity and gravity have been exploited to convey and to arrange the spheres.

The capillary deposition method does not have special requests to the environment conditions and can be varied to produce opal films with different thickness. The crack arrangement in films made from stable suspensions can be controlled by modifying the capillary cell.

The setup is also useful for the infiltration of an opal film with a liquid precursor. Inverse titania opal films with skeleton structure have been obtained after calcination.

Acknowledgment. Kind assistance from U. Wilczok is gratefully acknowledged. This work was supported by the Fonds der Chemischen Industrie and the German Science Foundation.

Supporting Information Available: UV-vis spectrum of a wet film 270 nm PS spheres in the capillary cell and high-resolution version of Figure 4D. This material is available free of charge via the Internet at http://pubs.acs.org.

References and Notes

(1) Yablonovitch, E. *Phys. Rev. Lett.* **1987**, *58*, 2059.
(2) John, S. *Phys. Rev. Lett.* **1987**, *58*, 2486.
(3) Talapin, D. V.; Shevchenko, E. V.; Kornowski, A.; Gaponik, N.; Haase, M.; Rogach, A. L.; Weller, H. *Adv. Mater.* **2001**, *13*, 1868.
(4) Pieranski, P. *Contemp. Phys*. **1983**, *24*, 25.
(5) Davis, K. E.; Russel, W. B.; Glantschnig, W. J. *J. Chem. Soc., Faraday Trans.* **1991**, *87*, 411.
(6) Mayoral, R.; Requena, J.; Moya, J. S.; Lopez, C.; Cintas, A.; Miguez, H.; Meseguer, F.; Vazquez, L.; Holgado, M.; Blanco, A. *Adv. Mater*. **1997**, *9*, 257.
(7) Clark, N. A.; Hurd, A. J.; Ackerson, B. J. *Nature* **1979**, *281*, 57.
(8) Okubo, T. *Langmuir* **1994**, *10*, 1695.
(9) Denkov, N. D.; Velev, O. D.; Kralchevshy, P. A.; Ivanov, I. B.; Yoshimura, H.; Nagayama, K. *Langmuir* **1992**, *8*, 3183.
(10) Dushkin, C. D.; Nagayama, K.; Miwa, T.; Kralchevsky, P. A. *Langmuir* **1993**, *9*, 3695.
(11) Dekenv, N. D.; Velev, O. D.; Kralchevsky, P. A.; Ivanov, I. B.; Yoshimura, H.; Nagayama, K. *Nature* **1993**, *361*, 26.
(12) Jiang, P.; Bertone, J. F.; Hwang, K. S.; Colvin, V. L. *Chem. Mater.* **1999**, *11*, 2132.
(13) Vlasov, Y. A.; Bo, X.-Z.; Sturm, J. C.; Norris, D. J. *Nature* **2001**, *414*, 289.
(14) Goldenberg, L. M.; Wagnar, J.; Stumpe, J.; Paulke, B.; Gornitz, E. *Langmuir* **2002**, *18*, 3319.
(15) Wong, S.; Kitaev, V.; Ozin, G. A. *J. Am. Chem. Soc*. **2003**, *125*, 15589.
(16) Yang, S. M.; Miguez, H.; Ozin, G. A. *Adv. Funct. Mater*. **2002**, *12*, 425.
(17) Norris, D. J.; Arlinghaus, E. G.; Meng, L. L.; Heiny, R.; Scriven, L. E. *Adv. Mater.* **2004**, *16*, 1393.
(18) Lopez, C. *Adv. Mater*. **2003**, *15*, 1679.
(19) Griesebock, B.; Egen, M.; Zentel, R. *Chem. Mater*. **2002**, *14*, 4023.
(20) Joannopoulos, J. D. *Nature* **2001**, *414*, 257.
(21) Joannopoulos, J. D.; Meade, R. D.; Winn, N. *Photonic Crystals, Molding the Flow of Light*; Princeton University Press: Princeton, NJ, 1995.
(22) Park, S. H.; Qin, D.; Xia, Y. N. *Adv. Mater*. 1**998**, *10*, 1028.
(23) Sözuer, H. S.; Haus, J. W. *Phys. Rev. B* **1992**, *45*, 139622.
(24) Blanco, A.; Chomski, E.; Grabtchak, S.; Ibisate, M.; John, S.; Leonard, S. W.; Lopez, C.; Meseguer, F.; Miguez, H.; Mondia, J. P.; Ozin, G. A.; Toader, O.; van Driel, H. M. *Nature* **2000**, *405*, 437.
(25) Wijnhoven, J. E. G. J.; Vos, W. L. *Science* **1998**, *281*, 802.
(26) Jiang, P.; Hwang, K. S.; Mittleman, D. M.; Bertone, J. F.; Colvin, V. L. *J. Am. Chem. Soc.* **1999**, *121*, 11630.
(27) Wijnhoven, J. E. G. J.; Bechger, L.; Vos, W. L. *Chem. Mater*. **2001**, *13*, 4486.
(28) Marlow, F.; Dong, W. T. *ChemPhysChem* **2003**, *4*, 549.
(29) Dong, W. T.; Bongard, H.; Tesche, B.; Marlow, F. *Adv. Mater*. **2002**, *14*, 1457.
(30) Dong, W. T.; Bongard, H. J.; Marlow, F. *Chem. Mater*. **2003**, *15*, 568.
(31) Dufresne, E. R.; Corwin, E. I.; Greenblatt, N. A.; Ashmore, J.; Wang, D. Y.; Dinsmore, A. D.; Cheng, J. X.; Xie, X. S.; Hutchinson, J. W.; Weitz, D. A. *Phys. Rev. Lett*. **2003**, *22*, 224501.
(32) Allain, C.; Limat, L. *Phys. Rev. Lett*. **1995**, *15*, 2981.
(33) Bergna, H. E. In *The Colloid Chemistry of Silica*; Bergna, H. E., Ed.; American Chemical Society: Washington, DC, 1994; Vol. 234, p376.